NEOPLASIA
www.neoplasia.com
Volume 19 Number 6 June 2017 pp. 460–470 460

Trabectedin and Campthotecin Synergistically Eliminate Cancer Stem Cells in Cell-of-Origin Sarcoma Models[1]

Lucia Martinez-Cruzado[*,†], Juan Tornin[*,†], Aida Rodriguez[*], Laura Santos[*], Eva Allonca[*,†], Maria Teresa Fernandez-Garcia[‡], Aurora Astudillo[§], Juana Maria Garcia-Pedrero[*,†,¶] and Rene Rodriguez[*,†,¶]

[*]Hospital Universitario Central de Asturias – Instituto de Investigación Sanitaria del Principado de Asturias, Oviedo, Asturias; [†]Instituto Universitario de Oncología del Principado de Asturias, Oviedo, Spain; [‡]Unidad Histopatología Molecular en Modelos Animales de Cáncer, IUOPA, Universidad de Oviedo, Oviedo, Spain; [§]Servicio de Anatomía Patológica, Hospital Universitario Central de Asturias, Oviedo, Spain; [¶]CIBER en oncología (CIBERONC), Madrid, Spain

Abstract

Trabectedin has been approved for second-line treatment of soft tissue sarcomas. However, its efficacy to target sarcoma initiating cells has not been addressed yet. Here, we used pioneer models of myxoid/round cell liposarcoma (MRCLS) and undifferentiated pleomorphic sarcoma (UPS) developed from transformed human mesenchymal stromal/stem cells (MSCs) to evaluate the effect of trabectedin in the cell type responsible for initiating sarcomagenesis and their derived cancer stem cells (CSC) subpopulations. We found that low nanomolar concentrations of trabectedin efficiently inhibited the growth of sarcoma-initiating cells, induced cell cycle arrest, DNA damage and apoptosis. Interestingly, trabectedin treatment repressed the expression of multiple genes responsible for the development of the CSC phenotype, including pluripotency factors, CSC markers and related signaling pathways. Accordingly, trabectedin induced apoptosis and reduced the survival of CSC-enriched tumorsphere cultures with the same efficiency that inhibits the growth of bulk tumor population. *In vivo*, trabectedin significantly reduced the mitotic index of MRCLS xenografts and inhibited tumor growth at a similar extent to that observed in doxorubicin-treated tumors. Combination of trabectedin with campthotecin (CPT), a chemotherapeutic drug that shows a robust anti-tumor activity when combined with alkylating agents, resulted in a very strong synergistic inhibition of tumor cell growth and highly increased DNA damage and apoptosis induction. Importantly, the enhanced anti-tumor activity of this combination was also observed in CSC subpopulations. These data suggest that trabectedin and CPT combination may constitute a novel strategy to effectively target both the cell-of-origin and CSC subpopulations in sarcoma.

Neoplasia (2017) 19, 460–470

Abbreviations: MRCLS, myxoid/round cell liposarcoma; UPS, undifferentiated pleomorphic sarcoma; *CSC*, cancer stem cell; hBMSC, human bone marrow-derived mesenchymal stromal/stem cell; CPT, campthotecin; STS, soft tissue sarcomas; NER, nucleotide excision repair; DSB, double strand breaks; SSB, single strand breaks; CI, combination index; TGI, tumor growth inhibition.

Address all correspondence to: Rene Rodriguez, PhD, Laboratorio ORL–IUOPA, Hospital Universitario Central de Asturias and Instituto Universitario de Oncología del Principado de Asturias, Av. de Roma s/m, 33011, Oviedo, Spain.
E-mail: renerg@ficyt.es, renerg.finba@gmail.com

[1]Funding: This work was supported by the Agencia Estatal de Investigación (AEI) [MINECO/Fondo Europeo de Desarrollo Regional (FEDER) (SAF-2013-42946-R and SAF-2016-75286-R to R.R.), ISC III/FEDER (Miguel Servet Program CP11/00024 and CPII16/00049 to R.R. and PI13/00259 and PI16/00280 to J.M.G-P) and Consorcio CIBERONC CB16/12/00390 to R.R and J.M.G-P)] and the Plan de Ciencia Tecnología e Innovación del Principado de Asturias (GRUPIN14–003) to R.R and J.M.G-P.
Received 16 February 2017; Revised 21 March 2017; Accepted 24 March 2017

1476-5586
http://dx.doi.org/10.1016/j.neo.2017.03.004

Introduction

Recent advances in sarcoma genomics have contributed to the development of new therapeutic strategies. However, cytotoxic drugs like doxorubicin alone or in combination with ifosfamide, remain as the most utilized agents for first-line treatment of soft tissue sarcomas despite their limited clinical response [1]. A hypothesis to explain the resistance of sarcomas to chemotherapy is the existence of subpopulations of drug-resistant cancer stem cells (CSCs), considered to be responsible for relapses and metastasis. It has been recently established that transformed MSCs and/or their immediate lineage progenitors are the most likely cell-of-origin for sarcomas [2,3]. Accordingly, many efforts have been undertaken to produce models of sarcomas based on MSCs transformed with relevant oncogenic events. This kind of models constitutes unparalleled systems to unravel the mechanisms underlying sarcomagenesis from the cell of origin, to explore the evolution of CSCs subpopulations and to search for CSC-specific therapies. In this regard, we have recently established and characterized pioneer models of undifferentiated pleomorphic sarcoma (UPS) and myxoid/round cell liposarcoma (MRCLS) developed from sequentially mutated human bone marrow-derived MSCs (hBMSCs) [4–6].

Trabectedin (ET-743, Yondelis) is a marine alkaloid originally isolated from the tunicate *ecteinascidia turbinate*. This compound has shown a consistent activity in soft tissue sarcomas (STS) in several clinical trials. Although, it has not demonstrated an objective advantage over first-line standard doxorubicin-based therapy, trabectedin has been approved for the treatment of adult patients with advanced STS, after failure of anthracyclines and ifosfamide, or those who are unsuited to receive these agents [1,7,8]. Trabectedin presents a complex mechanism of action affecting several key processes in both tumor cells and microenvironment [8–10]. Unlike classical alkylating drugs, trabectedin binds covalently to specific triplets of the DNA minor groove leading to a distortion of the double helix structure. These DNA adducts interfere with the binding of several transcription factors to their specific promoter elements. Specifically, trabectedin blocks the transcriptional activity of oncogenic transcription factors such as FUS-CHOP or EWS-FLI-1, which are products of characteristic chromosomal translocations respectively observed in MRCLS and Ewing's sarcoma [9,11–13]. Indeed, trabectedin is particularly efficient in MRCLS patients [14]. In MRCLS pre-clinical models, FUS-CHOP activity inhibition by trabectedin promotes adipogenic differentiation [12,15,16] and inhibits the production of inflammatory mediators by the tumor cells [17]. The structural changes induced by trabectedin cannot be resolved by the nucleotide excision repair (NER) mechanism, which instead are involved in the formation of double strand breaks (DSB) that could be repaired by homologous recombination repair [18–21]. Therefore, trabectedin exhibits reduced efficacy in cells deficient in NER, while it is more potent in homologous recombination repair-deficient cells [22–24]. The formation trabectedin-DNA adducts are also able to trap DNA topoisomerase I, which normally introduce single strand breaks (SSB) to relax DNA supercoiling during replication and transcription. Thus, trabectedin-induced topisomerase I-DNA complexes mediate SSB formation that may evolve to DSB [25].

Several combination strategies have been tested in order to increase the therapeutic index of trabectedin in sarcomas. Many of these strategies are based on the combination with compounds that induce DNA damage while also interfering with DNA damage repair mechanisms, such as doxorubicin, cisplatin, PARP inhibitors or campthotecins [1,8,21,26–28]. Campthotecin (CPT) and its derivatives irinotecan and topotecan are chemotherapeutic drugs with proved activity against several types of sarcoma [29–32]. CPT targets DNA topoisomerase I and inhibits its resealing activity leading to the stabilization of the transiently-generated SSB which can be converted into toxic DSB by collision with replication or transcription complexes [33,34].

In this report, we show that trabectedin inhibits tumor cell growth initiated by cell-of-origin models of MRCLS and UPS, represses the expression of important genes associated to the CSC phenotype and targets CSC subpopulations at rates comparable to that of non-CSC subpopulations. Furthermore, we show that trabectedin efficacy is synergistically increased by combination with CPT.

Materials and Methods

Cell Types and Drugs

Previously developed transformed human BM-MSCs lines (Table S1 and Supplemental information) were cultured as previously described [4–6,35]. Trabectedin and camptothecin were obtained from PharmaMar (Madrid, Spain) and Sigma (St Louis, MO), respectively (Supplemental information). All experimental protocols have been performed in accordance with institutional review board guidelines and were approved by the Institutional Ethics Committee of the Hospital Universitario Central de Asturias. All samples from human origin were obtained upon signed informed consent.

Western Blot

Whole cell protein extraction and Western blot analysis were performed as previously described [36]. Antibodies used are described in Supplemental information.

RT-qPCR Assays

The Human Cancer Stem Cells RT2 Profiler PCR Array (PAHS-176-Z; SA Biosciences, Qiagen Iberia, Madrid, Spain) was used to analyze the expression of 84 genes linked to CSCs properties according to the manufacturer instructions and as described before [37,38]. A complete data set including gene information and experimentally obtained C_t values is presented in Table S2.

Cell Viability Assays

The viability of all cell lines in the presence and absence of drugs was determined using the cell proliferation reagent WST-1 (Roche, Mannheim, Germany) as described before [38]. In dose–response experiments cells were treated for 72 hours and all the assayed conditions contain the same concentration of drug solvent (DMSO). The concentration of half-maximal inhibition of viability (IC_{50}) for each treatment was determined by non-linear regression. The existence of synergy in drug combinations was determined by calculating the combination index (CI) according to the Chou and Talalay method using CompuSyn software (ComboSyn) [39]. CI *vs.* the fraction affected (F_a) plots were generated for six combinations of drugs at a fixed ratio according to their IC_{50}s. CI values indicate synergistic (<1), additive (=1) and antagonistic (>1) drug interactions.

Tumorsphere Culture

Tumorsphere formation protocol and the analysis of the effects of drugs on tumorsphere formation ability were previously described [38].

Immunofluorescence Staining

In immunofluorescence staining experiments in adherent cultures (2-D) and tumorspheres (3-D) fixation, staining and mounting of the samples were performed as previously reported [38]. Antibodies and experimental conditions are described in Supplemental information.

Cell-cycle Analysis

Cell-cycle analysis of floating and adherent cells was carried out as described previously [34].

Aldefluor Assay

ALDH activity was determined using the activated Aldefluor™ reagent (Stem Cells Technologies, Grenoble, France) as previously reported [37].

Soft Agar Colony Formation Assay

A soft agar colony formation assay was carried out using the CytoSelect™ 96-Well Cell Transformation Assay Kit (Cell Biolabs Inc., San Francisco, CA) as described [37] (Supplemental information).

Xenograft Experiments

Female NOD/SCID mice of 5–6 weeks old (Janvier Labs, St Berthevin, France) were inoculated subcutaneously (s.c.) with $1{\times}10^6$ T5H–FC#1 cells. Once tumors reached 200–500 mm3, the mice were randomly assigned to receive intra-venous (i.v.) treatments of saline solution (control) or trabectedin at a dose of 0.15 mg/kg on days 0, 7, 14, and 18. Mean tumor volume differences between groups were determined using a caliper. Animals were sacrificed by CO_2 asphyxiation on day 19 after the start of treatments and the tumors were extracted and weighed. The Student *t* test was performed to determine the statistical significance between control and treated groups. Survival was represented using Kaplan–Meier analysis and the log-rank test to estimate significant differences among groups (PAST 3.01 software). Drug efficacy was expressed as the percentage tumor growth inhibition (%TGI) calculated as previously reported [38]. All animal research protocols were approved by the Animal Research Ethical Committee of the University of Oviedo prior to the study.

Histological Analysis

Tumor samples were fixed in formol, embedded in paraffin, cut into 4-μm sections, and stained with hematoxylin and eosin (H&E) [40]. Quantification of mitosis was performed by counting the number of mitotic figures per 10 high power fields (40×). Tumor grade was analyzed in H&E-stained preparations using a variant of the French Federation of Comprehensive Cancer Centers grading system (Supplemental information).

Results

Antiproliferative Effects of Trabectedin

We have previously developed UPS (MSC-5H-GFP, MSC-5H-O, T-5H-GFP#1 and T-5H-O cell lines) and FUS-CHOP-expressing MRCLS models (MSC-5H-FC and T-5H-FC#1 cell lines) using hBMSCs sequentially mutated with up to six oncogenic events (see Table S1 and Supplemental information for a description of these cell lines) [4–6]. First, in 72 hours-treatment dose–response experiments, we compared the cytotoxic effect of trabectedin on these cell-of-origin models with that observed in wild type hBMSCs and other tumor cell lines (Figure 1*A*). Wild-type hBMSCs and the lung cancer cell line A-549 were respectively fully and partially resistant to trabectedin. On the other hand, the MRCLS cell line 402.91 was the most sensitive cell line. The sarcoma-initiating cells MSC-5H-GFP, MSC-5H-FC, their xenograft-derived cell lines T5H–GFP#1 and T5H–FC#1 and the MRCLS cell line 1765 were also sensitive to low nanomolar concentrations of trabectedin, although display IC50 values between five and ten times higher than the 402.91 cell line (Figure 1*A*). In addition, time-course experiments showed a time-dependent decrease in cell viability of the cell-of-origin models treated with 4 nM trabectedin (Figure 1*B*). To further investigate the mechanism underlying the antiproliferative effect of trabectedin, we examined the effect of this drug on the cell cycle distribution, DNA damage induction and apoptosis induction. Both MSC-5H-FC (Figure 1*C*) and T-5H-FC#1 cells (Figure S1*A*) treated with 0.5 nM trabectedin showed a slow transition through the S-phase followed by G2 arrest, meanwhile cells treated with a higher concentration (2 nM) showed a more stringent S-phase block and a consistent increment in the Sub-G1 apoptotic population at latter times. In addition, trabectedin was also a potent inducer of DSBs in these cell lines as indicated by the dose-dependent increase in both intranuclear H2AX foci and protein levels after 1 hour treatment (Figure 1, *D–F*, Figure S1, *B* and *C* and Figure S2). In line with these results, both UPS model (MSC-5H-GFP/ T5H–GFP#1) and MRCLS model (MSC-5H-FC/ T5H–FC#1) cell types displayed a similar time-dependent apoptotic PARP cleavage after trabectedin treatment (Figure 1*G*). Thus, trabectedin induced cell cycle arrest and DNA damage followed by apoptotic cell death in cell-of-origin sarcoma models.

Trabectedin Down-Regulates the Expression of Genes Associated to the CSC Phenotype

To know how trabectedin affected the CSC phenotype in sarcoma development, we performed RT-PCR in T-5H-FC#1 MRCLS-forming cells treated for 24 h with 1 nM trabectedin to analyze the expression of an array of 84 genes with well-known functions in pluripotency, self-renewal, migration, metastasis, and signal transduction in CSCs as well as several CSC markers. Trabectedin led to statistically significant changes (fold change ≥2; $P < .05$) in the expression of 36 genes (Figure 2, *A* and *B*). Notably, this drug induced the down-regulation of almost all the altered genes (3 up-regulated genes and 33 down-regulated genes). These repressed genes included various important pluripotency factors like SOX2, C-MYC, KLF4, and BMI1, CSC markers in different types of tumors, including sarcomas, like ABCG2, KIT/CD117, MUC1 and GATA3 and genes involved in relevant stemness signaling pathways such as NOTCH signaling (MALML1 and JAG1) or NFκB signaling (NFκB1 and IκBKB) among others (Figure 2*B*). In striking contrast, we previously showed that after the treatment of T5H–FC#1 cells with the chemotherapeutic drug doxorubicin, commonly used in the treatment of soft tissue sarcomas, most of the statistically altered CSC-related genes resulted up-regulated (21 up-regulated genes and 9 down-regulated genes) [38]. Among the doxorubicin-up-regulated genes there are relevant pluripotency factors and/or CSC markers like NANOG, POU5F1/OCT3/4, THY1/ CD90, ALDH1A1, PROM1/CD133, KIT/CD117 or CD24 [38].

These data suggest that trabectedin treatment may disadvantage the CSC phenotype in sarcomas.

Trabectedin Targets CSC Subpopulations In Vitro

All the sarcoma-initiating cells used in this study were able to form tumorspheres with enhanced tumor formation ability, as previously shown [37]. To test whether trabectedin may affect CSC viability, MSC-5H-FC and T-5H-FC#1 cells were treated with increasing concentrations of trabectedin for 72 h and then grown under CSC culture conditions to assay the ability of trabectedin to inhibit the

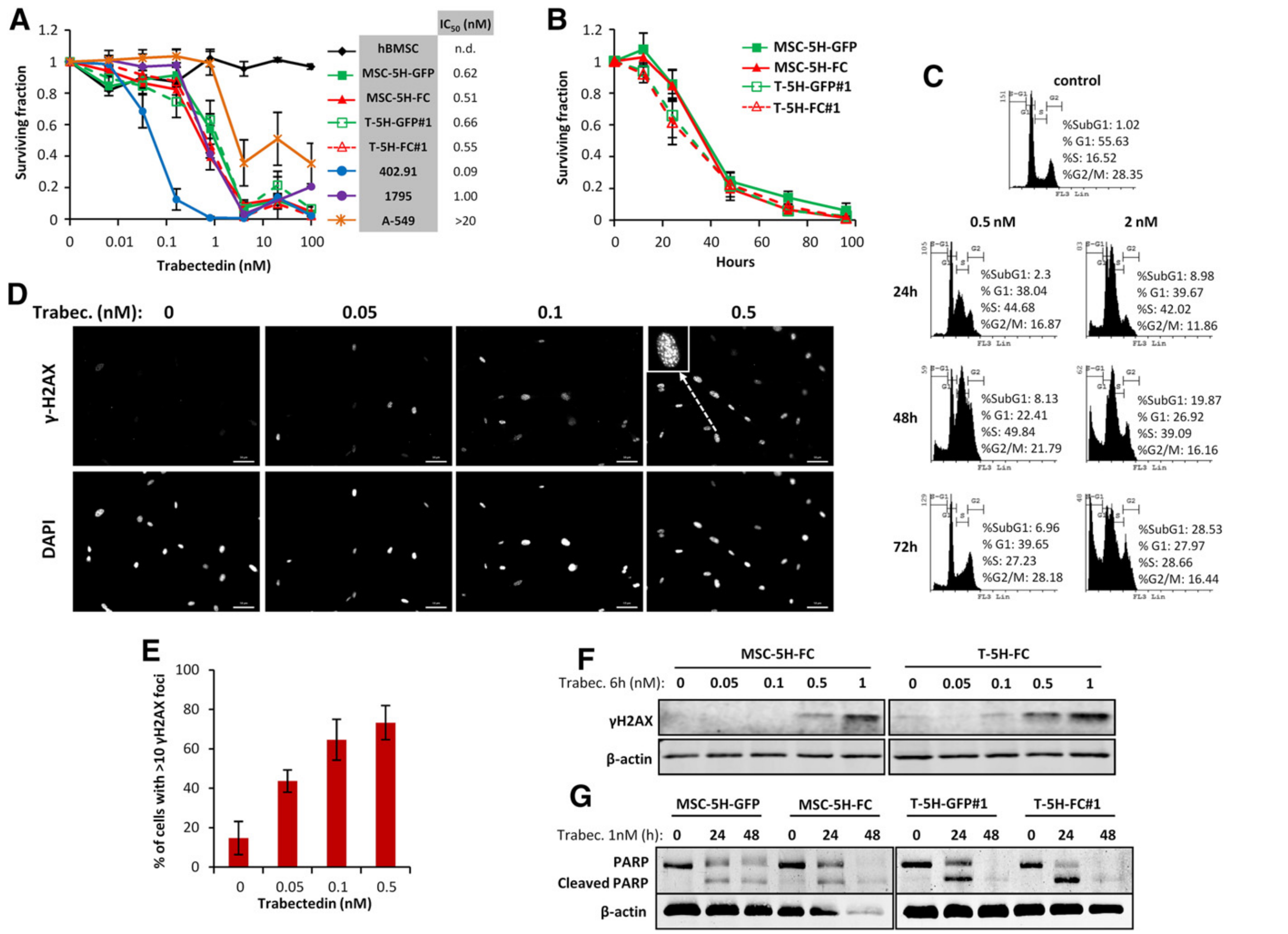

Figure 1. Antiproliferative effects of trabectedin. (A-B) Cell viability (WST1 assay) measured after the treatment of the indicated cell lines with increasing concentrations of trabectedin for 72 hours (A) or with 4 nM trabectedin for the indicated time-course (B). IC_{50} values for each cell type are shown (A). (C) Time-course evolution of the cell cycle distribution of MSC-5H-FC cells treated with the indicated concentrations of trabectedin. (D) Representative images of immunostaining experiments showing a dose-dependent increase in γH2AX foci formation following 1 hour trabectedin treatment in MSC-5H-FC cells. Inset shows a magnification of a representative cell. Scale bars = 50 μm. An enlarged color version of this panel is displayed as Figure S2. (E) Quantification of γH2AX foci was performed by counting more than 200 cells in each condition. The percentage of cells presenting high level of DNA damage (>10 foci) is displayed. A similar set of experiments for T-5H-FC#1 cells is presented as Figure S1, *B* and *C*. (F) Western blotting showing γH2AX protein levels after the indicated trabectedin treatment. (G) Western blotting using an antibody to recognize normal and apoptotic-cleaved forms of PARP in the indicated cell lines treated with 1 nM trabectedin for the indicated times. β-Actin levels were used as loading control in Western blotting experiments. Error bars represent the standard deviation of at least 12 replicates from three independent experiments.

formation of tumorspheres. Trabectedin efficiently reduced both the number (Figure 3*A*) and viability (Figure 3*B*) of tumorspheres, showing IC_{50} values similar to those obtained after the treatment of adherent cultures (Figure 1*A*). These results suggest that trabectedin is able to effectively target CSCs subpopulations (tumorsphere-forming subpopulations) *in vitro* with the same efficiency that inhibits the growth of bulk tumor population. To confirm the effect of trabectedin on CSCs we directly treated already formed tumorspheres with this drug for 72 hours [38]. After trabectedin treatment, MSC-5H-FC and T5H–FC#1 tumorspheres were smaller and displayed a disrupted and irregular morphology and the number and viability of the tumorspheres dramatically decreased in a dose-dependent fashion in both cell types (Figure 3, *C–E*). Consistent with this findings trabectedin was able to induce dose-dependent apoptosis in tumorsphere-forming cells, as shown by PARP apoptotic cleavage induction *in situ* (Figure 3*F*). In fact, trabectedin induced similar levels of apoptosis in bulk-adherent and CSC-tumorsphere cultures as shown in dose–response and time-course experiments (Figure 3, *G–H*). In addition, trabectedin caused a similar degree of DNA damage in adherent and tumorsphere cultures as seen by the increase in γH2AX levels (Figure 3*I*).

Tumorsphere cultures of these sarcoma models are highly enriched in Aldefluor activity. Importantly, the subpopulation of T-5H-O cells with high Aldefluor activity ($ALDH^{high}$) displayed increased tumorigenic properties, thus validating this activity as a CSC marker in our cells [37]. To analyze the effect of trabectedin on this subpopulation of CSCs, we isolated $ALDH^{high}$ and $ALDH^{low}$ T-5H-O cells by flow cytometry and put them back in adherent cultures. As expected, these subpopulations showed relevant differences in Aldefluor activity (Figure 4*A*) and expressed higher levels of the ALDH1 isoforms ALDH1A1 and ALDH1A3 (Figure 4*B*). In addition, both subpopulations were equally sensitive to 72 hours-treatment with increasing concentrations of

A

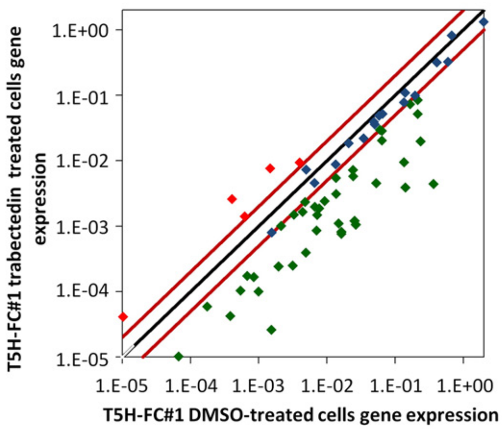

B

Gene expression altered by trabectedin					
Gene symbol	fold regulation	pvalue	Gene symbol	fold regulation	pvalue
SNAI1	6.46	2.06E-03	ATXN1	-5.07	5.44E-03
THY1	5.21	8.20E-03	PTCH1	-6.53	9.25E-04
PTPRC	4.01	7.17E-03	WEE1	-8.17	4.09E-02
ITGA6	-2.00	2.00E-02	KIT	-8.99	2.24E-03
MUC1	-2.11	1.43E-02	FZD7	-9.85	5.72E-03
EPCAM	-2.19	3.68E-02	GSK3B	-11.56	8.42E-04
BMI1	-2.21	1.46E-02	JAG1	-11.87	4.85E-04
ITGA2	-2.52	1.35E-04	JAK2	-12.39	9.52E-03
ABCG2	-2.66	5.00E-02	LIN28B	-12.59	5.37E-03
LIN28A	-2.96	1.51E-02	TWIST1	-13.46	1.32E-02
DNMT1	-3.13	6.22E-04	ID1	-14.19	7.62E-05
CHEK1	-3.31	7.62E-04	SIRT1	-19.88	1.07E-02
ERBB2	-3.35	4.35E-02	NFKB1	-21.04	2.56E-03
TAZ	-3.80	8.87E-03	MAML1	-21.37	1.08E-04
EGF	-3.90	2.89E-05	KLF4	-25.00	2.04E-04
LATS1	-4.11	4.07E-03	SOX2	-58.59	2.53E-05
IKBKB	-4.18	1.06E-02	MYC	-82.16	1.57E-04
KITLG	-4.36	5.24E-03	GATA3	-86.43	1.23E-02

Figure 2. Changes in CSC-related gene expression induced by trabectedin. RNA isolated from T5H–FC#1 cells treated with the carrier substance (DMSO) or with 1 nM trabectedin for 24 hours was used to analyze the expression of 84 CSC-related genes (RT^2 Profiler™ PCR Array System PAHS-176Z, Qiagen). (A) Scatter plot representing the expression values in control (DMSO) and trabectedin-treated cells for each gene. Genes above and below the dashed lines are expressed more than two-fold up or down in treated *versus* untreated cells respectively. (B) List of genes differentially expressed (fold change ≤2 or ≥2 and *P* value (two-sided Student *t* test) < 0.05) after trabectedin treatment.

trabectedin (Figure 4*C*). Even though the ability to form colonies in soft agar, a surrogate *in vitro* transformation assay, was higher in ALDH^{high} cells, trabectedin pre-treatment robustly prevented colony formation in both subpopulations (Figure 4*D*). Likewise, trabectedin pre-treatment completely abolished the ability of both subpopulations to grow as tumorspheres (Figure 4*E*). In line with these observations, trabectedin induced apoptosis (PARP cleavage) and DNA damage (increase in γH2AX protein levels) with similar efficacy in ALDH^{high} and ALDH^{low} subpopulations (Figure 4*B*). Altogether these results support that trabectedin could constitute an effective treatment to target both CSC and non-CSC subpopulations in sarcoma.

Trabectedin Inhibits the Growth of MRCLS Xenografts

Trabectedin treatment caused an important tumor growth inhibition in MRCLS xenografts originated from T-5H-FC#1 cells. Compared to vehicle (saline buffer) treated group, trabectedin treated mice (0.15 mg/kg on days 0, 7, 14, and 18) showed significant differences in tumor volume as soon as 7 days after the beginning of the treatment (Figure 5*A*). At later times, trabectedin-induced TGI percentages rose up to 54.16%, and treated mice showed a significant increase in survival (Figure 5, *A* and *B*). Likewise, tumor weights in the control series doubled those of the trabectedin-treated series at the end of the experiment (Figure 5*C*). Notably, trabectedin treatment did not cause loss of weight (Figure 5*D*) or other adverse effects. The anti-tumor activity of trabectedin is similar to that previously reported after the treatment of T-5H-FC#1 xenografts with doxorubicin (6 mg/kg on days 0, 7, and 14), although this treatment resulted toxic at later time points [38] (see Figure S3 for a comparison of trabectedin and doxorubicin treatments).

Histological examination of T-5H-FC#1 derived tumors showed that trabectedin-treated tumors exhibited significantly lower mitotic counts than untreated tumor samples (Figure 5, *E* and *F*). Furthermore, tumors treated with trabectedin showed a significant reduction in tumor grade (Figure 5*G*).

Trabectedin and Camptothecin Combination Shows Synergistic Cytotoxic Effect

In an effort to increase the anti-tumor effect of trabectedin in sarcoma-initiating cells, we combined this drug with CPT. Since both drugs are potent inducers of DSBs by two different mechanisms and alkylating agents have been shown to increase the anti-tumor activity of campthotecins [41,42] we hypothesized that they could synergize to inhibit tumor cell growth.

MSC-5H-FC and T-5H-FC#1 cells were moderately sensitive to CPT presenting IC_{50} values of 5.3 and 8.9 nM respectively (Figure S4*A*). Combination of trabectedin with increasing concentrations of CPT markedly increased the cytotoxicity of trabectedin in both cell types even at very low concentrations of CPT (Figure 6, *A* and *B*). By representing the data of the combination normalized to effect of CPT alone we found that CPT 0.5 nM shifted the IC_{50} of trabectedin from 0.51 to 0.029 nM in MSC-5H-FC cells and from 0.55 to 0.017 nM in T-5H-FC#1 cells (Figure 6, *C* and *D*). To test whether the trabectedin and CPT combination has a synergistic cytotoxic effect we calculated their CI using the CompuSyn software according to the Chou-Talalay method [39]. In 72 hours-treatment experiments all assayed constant ratio combinations showed CI values far below 1 in both MSC-5H-FC and T-5H-FC#1 cells with CI values for ED_{50} combination doses of 0.041 and 0.024, respectively (Figure 6, *E* and *F*). Therefore these data meet the criteria for very strong synergism (CI <0.1) between these drugs. In line with this synergistic effect the combination of low concentrations of trabectedin and CPT induced significantly higher levels of γH2AX foci and protein levels and apoptotic PARP cleavage than either drug alone (Figure 6, *G–I* Figure S4*B* and Figure S5). Importantly pretreatment with the drug combination was much more efficient in reducing the ability of MSC-5H-FC and T-5H-FC#1 cells to grow tumorspheres than trabectedin or CPT alone (Figure 6, *J* and *K*). In addition direct treatment of the tumorspheres formed by both cell types with the

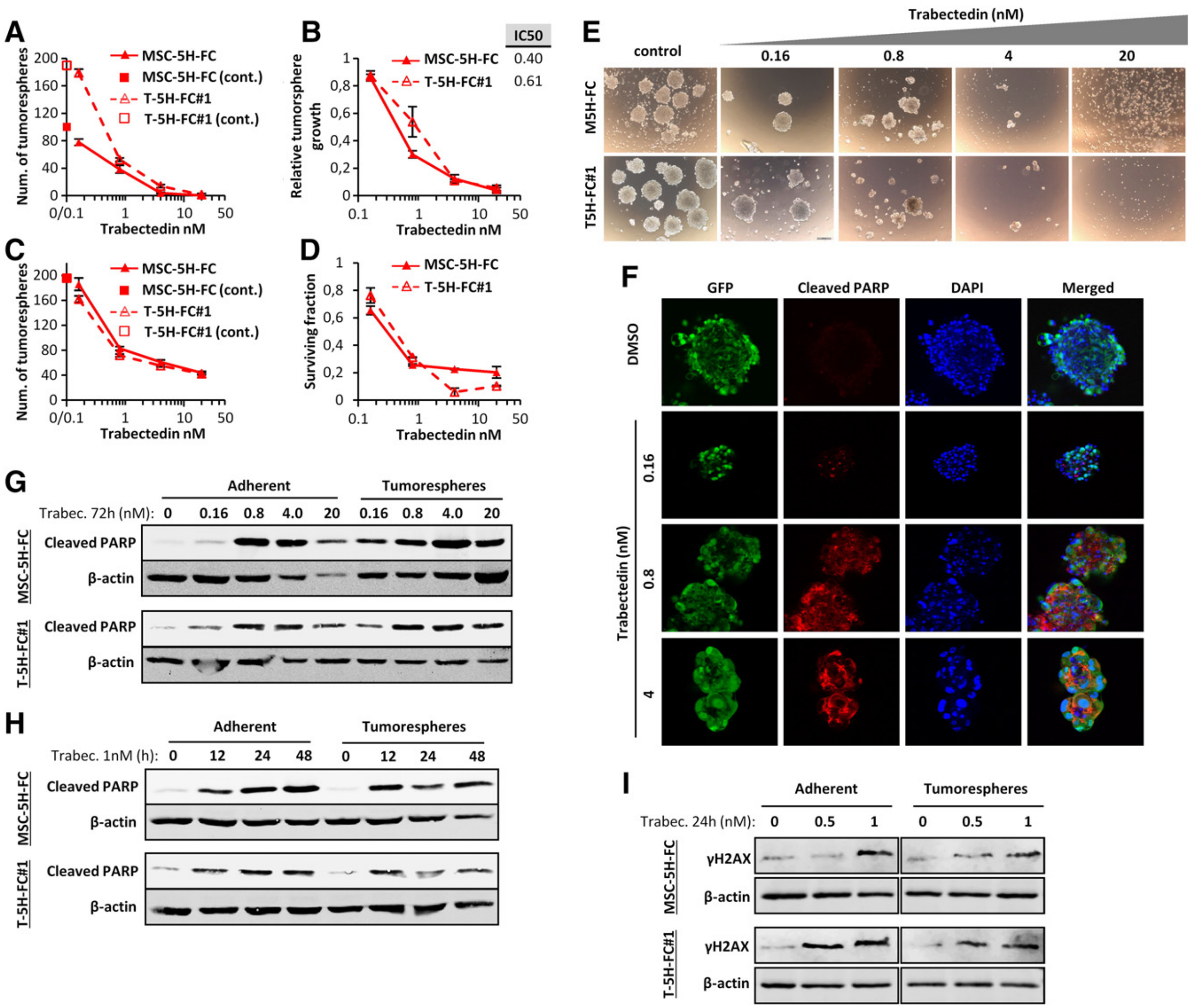

Figure 3. Trabectedin targets CSC-enriched tumorsphere cultures. (A-B) MSC-5H-FC and T-5H-FC#1 cell lines treated with the indicated concentrations of trabectedin for 72 hours were grown in tumorsphere culture conditions for 10 days. After this period, the number (represented as % of control) (A) and the cell viability (WST1 assay) (B) of tumorspheres formed were measured. (C-E) Counting (C), cell viability (D) and representative images (E) of the tumorspheres remaining after the direct treatment of tumorsphere cultures of MSC-5H-FC and T-5H-FC#1 cells with the indicated concentrations of trabectedin for 72 h. Scale bars = 200 μm. Error bars represent the standard deviation of at least three independent experiments. F) Detection of cleaved PARP in GFP-positive T5H–FC#1 sarcospheres treated with DMSO, or increasing concentrations of trabectedin for 72 h. Scale bars = 500 μm. (G-H) Western blot analysis showing the apoptotic cleavage of PARP in MSC-5H-FC and T-5H-FC#1 adherent and tumorsphere cultures after the indicated dose–response (G) and time-course (H) trabectedin treatments. I) Protein levels of γH2AX after the indicated trabectedin treatment in MSC-5H-FC and T-5H-FC#1 adherent and tumorsphere cultures. β-actin levels were used as loading control.

combination also resulted in enhanced tumorsphere disruption and cytotoxicity (Supplementary Figure S4, *C* and *D*). Moreover trabectedin and CPT combination is highly effective in boosting apoptotic PARP cleavage and γH2AX levels in CSC-enriched tumorsphere cultures (Figure 6*L*)

Altogether these results suggest that the combination of trabectedin and CPT has a synergistic cytotoxic effect on sarcoma initiating cells, including their CSC subpopulations.

Discussion

In this work we aim to investigate the effect of trabectedin on sarcoma-initiating. We previously found that tumorsphere cultures or ALDH^{high} cells isolated from our MRCLS model are enriched in *bona fide* subpopulations of CSCs [37]. Here we show that trabectedin is able to decrease survival, induce apoptosis and cause DNA damage in these CSCs subpopulations as efficiently as in unselected adherent cultures. To the best of our knowledge, this is the first work describing the effect of trabectedin on sarcoma CSC subpopulations. In other types of tumors it has been described that trabectedin is able to induce apoptosis and G2/M cell cycle arrest and to reduce tumorsphere growth in CSC subpopulations derived from prostate cancer cell lines [43]. We also demonstrate that, unlike what we previously reported for doxorubicin [38], trabectedin represses the expression of multiple genes and pathways involved in the development and maintenance of the CSC phenotype. Despite the differential effects of trabectedin and doxorubicin on the expression of genes related to the CSC phenotype, trabectedin treatment of

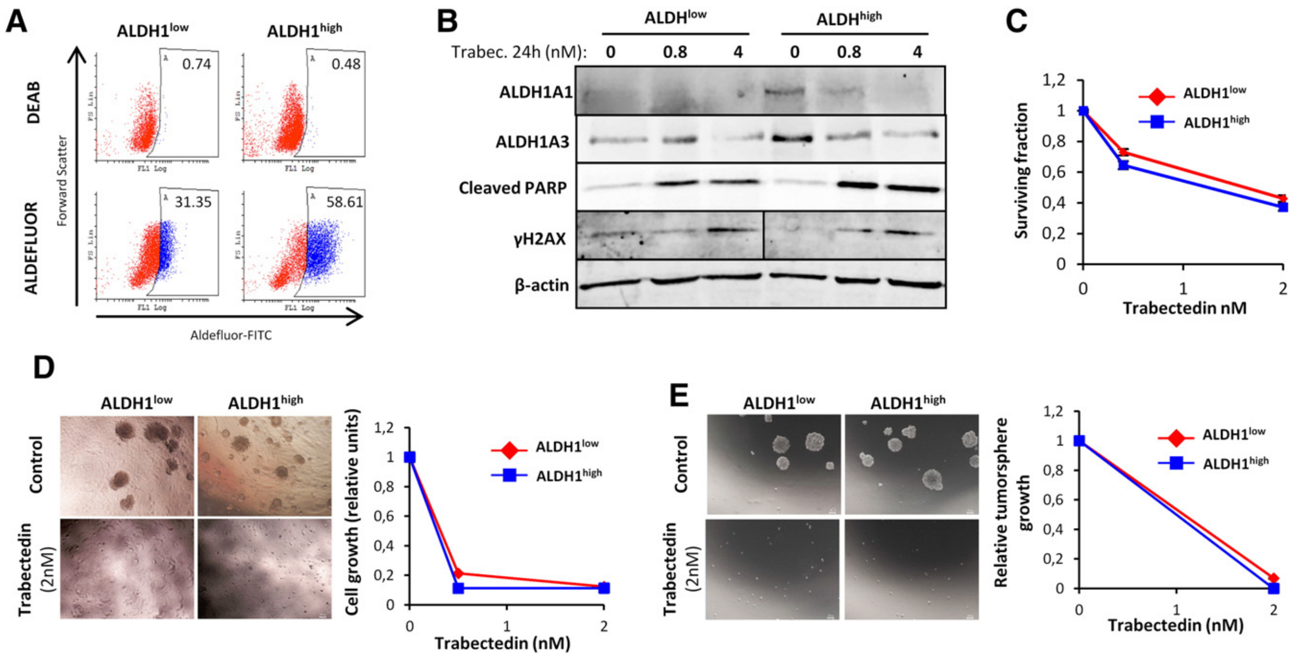

Figure 4. Trabectedin targets both ALDH1^{low} and ALDH1^{high} subpopulations. ALDH1^{low} and ALDH1^{high} subpopulations in T5H–O cells were sorted by flow cytometry and expanded for 24 h prior to start the experimental procedures. (A) ALDEFLUOR assay showing the activity of ALDH1 in ALDH1^{low} and ALDH1^{high} subpopulations just before starting trabectedin treatments. ALDH1 activity was blocked with the specific inhibitor DEAB to establish the basal level. (B) Protein levels of the indicated factors in ALDH1^{low} and ALDH1^{high} subpopulations treated with the indicated concentrations of trabectedin for 24 h. (C) Cell viability (WST1 assay) measured after the treatment of the subpopulations with increasing concentrations of trabectedin for 72 hours. (D-E) ALDH1^{high} and ALDH1^{low} subpopulations were pre-treated with the indicated concentrations of trabectedin for 24 h and assayed for soft agar colony formation (anchorage-independent growth) (D) and tumorsphere formation (E). Representative images (left panels) and relative quantification of the cell growth (WST-1 assay; right panels) are shown. Scale bars = 200 μm. Error bars represent the standard deviation of at least two independent experiments.

T-5H-FC#1-generated xenografts did not provide a therapeutic advantage over previously reported doxorubicin treatment of these xenografts [38] (Figure S3), thus reproducing the results observed in phase III clinical trials [44]. These data suggest that the toxicity of trabectedin may not be related with its ability to modulate CSC-related gene expression. In any case, new strategies with a further impact on CSC subpopulations are needed to improve the therapeutic efficacy of trabectedin over the standard treatments. Therefore, we aimed to find combination strategies that could improve the anti-tumor effects of trabectedin on both CSC and non-CSC subpopulations. We explored the combination of trabectedin with another DNA damaging agent CPT. Interestingly, a system biology approach showed a high degree of similarity between transcriptional signatures induced by trabectedin and irinotecan in a model of myelomonocytic leukemia, thus providing potential rationales to combine these drugs to obtain synergistic antitumor effects [45]. Indeed, the combination of trabectedin and CPT derivatives has proven anti-tumor synergistic effects in Ewing Sarcoma cells through a mechanism by which cells become hypersensitive to CPT by the trabectedin-induced down-regulation of EWS-FLI-1-mediated expression of the RecQ helicase Werner syndrome protein (WRN) [26]. In addition, this combination also resulted highly effective in the inhibition of a human rhabdomyosarcoma xenograft [28]. In 12 patients with advanced translocation-positive sarcomas, trabectedin followed by irinotecan treatment showed promising results since the treatment was well-tolerated and caused disease stabilization in five patients with Ewing sarcoma and a partial response in a patient with synovial sarcoma [46]. In another Ewing sarcoma patient, a similar combination regimen also resulted in disease stabilization before treatment-unrelated death occurred [47]. Moreover, the combination of trabectedin with irinotecan or topotecan demonstrated synergistic effects in ovarian clear cell carcinoma cells [48]. Altogether, trabectedin plus CPT combination seems to be a valuable strategy against different types of STS and possibly other solid tumors.

In this study, we proved that trabectedin plus CPT combination exhibits a very strong synergism in a model of MRCLS-initiating cells. Importantly, we also demonstrate that this combination is highly effective in eliminating CSC subpopulations. By comparing WRN expression in MSC-5H-GFP and MSC-5H-FC cells, we found that FUS-CHOP expression did not induce an up-regulation of this helicase (Figure S6*A*). However, treatment of MSC-5H-FC cells with trabectedin or CPT produced a dose-dependent inhibition of WRN protein levels. Moreover, the combination of both drugs induced a deeper repression of WRN expression (Figure S6*B*). In line with these results, it has been reported that CPT treatment may induces the degradation of WRN and this effect is related with the sensitivity of tumor cells to CPT [49]. These findings suggest that the profound down-regulation of WRN induced by trabectedin plus CPT treatment may play a role in the synergistic cytotoxic effect of this combination.

In addition, other mechanisms of synergism between trabectedin and CPT may be acting in our sarcoma models and other types of tumors. In this regard, other alkylating agents have been shown to increase the anti-tumor activity of campthotecins [41,42]. Mechanistically, the anti-tumor activity of alkylating agents seems to be in part mediated by toposimerase I trapping and enhancement of topoisomerase I cleavage complexes [42]. Interestingly, DNA

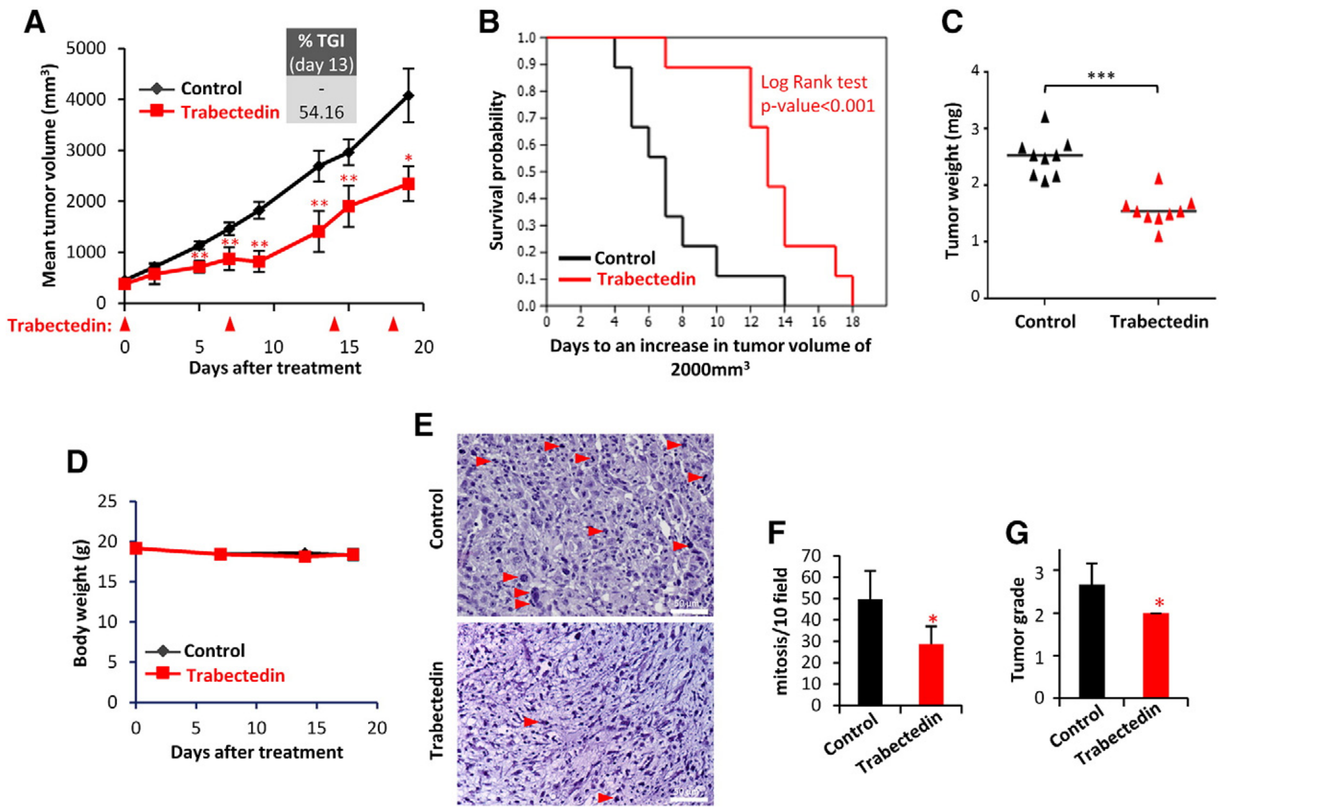

Figure 5. Trabectedin inhibits the growth of MRCLS sarcoma xenografts. Mice with established T-5H-FC#1 tumor xenografts were randomly assigned to two different groups (n = 10 *per* group) and treated i.v. with saline buffer (control) or trabectedin at a dose of 0.15 mg/kg on days 0, 7, 14, and 18. (A) Curves representing the mean tumor volume of T-5H-FC#1 xenografts during the treatments. Drug efficacy expressed as the percentage of TGI at day 13 is indicated. (B) Kaplan–Meier curves generated using the reaching of a tumor volume of 1000 mm^3 as end-point event. (C) Tumor weight (D) at the end of the experiment. (D) Body weights of mice during the treatments. (E) H&E staining of formalin-fixed paraffin embedded T5H–FC#1-generated xenografts extracted from control and trabectedin-treated mice. Mitotic cells (red arrows) are indicated. Scale bars = 50 μm. (F) Quantification of mitosis as the number of mitotic figures per 10 high power fields (40×). (G) Tumor grade score according to a variant of the French Federation of Comprehensive Cancer Centers system. Error bars represent the standard deviation and asterisks indicate statistically significant differences between trabectedin-treated and control groups (*:$P < .05$, **:$P < .005$, ***:$P < .0005$; two-sided Student *t* test). The log-rank test *P* value was used to estimate significant differences between control and drug treated groups in Kaplan–Meier analysis.

alkylation induced by trabectedin also mediates the formation of topoisomerase I cleavage complexes at sites different to those observed after CPT treatment [25]. Therefore, the combination could highly increase the formation of DNA breaks, ultimately leading to synergistic toxicity. Although the main mechanism of trabectedin-induced toxicity seems to be independent of topoisomerase I activity [50], it is plausible that in combination with CPT, the enhanced poisoning of this enzyme may become a relevant anti-tumor mechanism. Since WRN play an important role in the DNA damage response originated by topoisomerase I inhibition, the down-regulation of WRN by trabectedin and CPT may cooperate to increase the toxicity.

Another possible mechanism of synergy between both drugs may involve the ability of trabectedin to interfere with the NER mechanism by forming a ternary complex with DNA and the ERCC Excision Repair 5 (EERC5) endonuclease which eventually triggers the formation of DSBs [20]. The confluence of two different mechanisms of DSB generation could result in the accumulation of unresolved DNA damage, which may exceed the capacity of the cell to cope with DNA damage, consequently triggering a synergistic cytotoxic response.

Conclusion

These data suggest that trabectedin could act as an anti-pluripotency therapy able to effectively target both CSC and non-CSC populations derived from sarcoma initiating cells. Moreover, their efficacy is synergistically enhanced when combined with CPT, thus reinforcing the rationale for the clinical testing of this combination in STS sarcoma patients.

Supplementary data to this article can be found online at http://dx.doi.org/10.1016/j.neo.2017.03.004.

Conflict of Interest Disclosure Statement

The authors declare no competing financial interests.

Author Contributions

L.M-C, J.T & A.R: development of methodology, performance of experimental procedures, acquisition, analysis and interpretation of data. L.S & E.A: performance of experimental procedures. A.A & M-T.F-G: analysis and interpretation of data. J.M.G-P: analysis and interpretation of data and financial support. R.R: Conception and design, analysis and interpretation of data, and manuscript writing. The manuscript has been seen and approved by all authors.

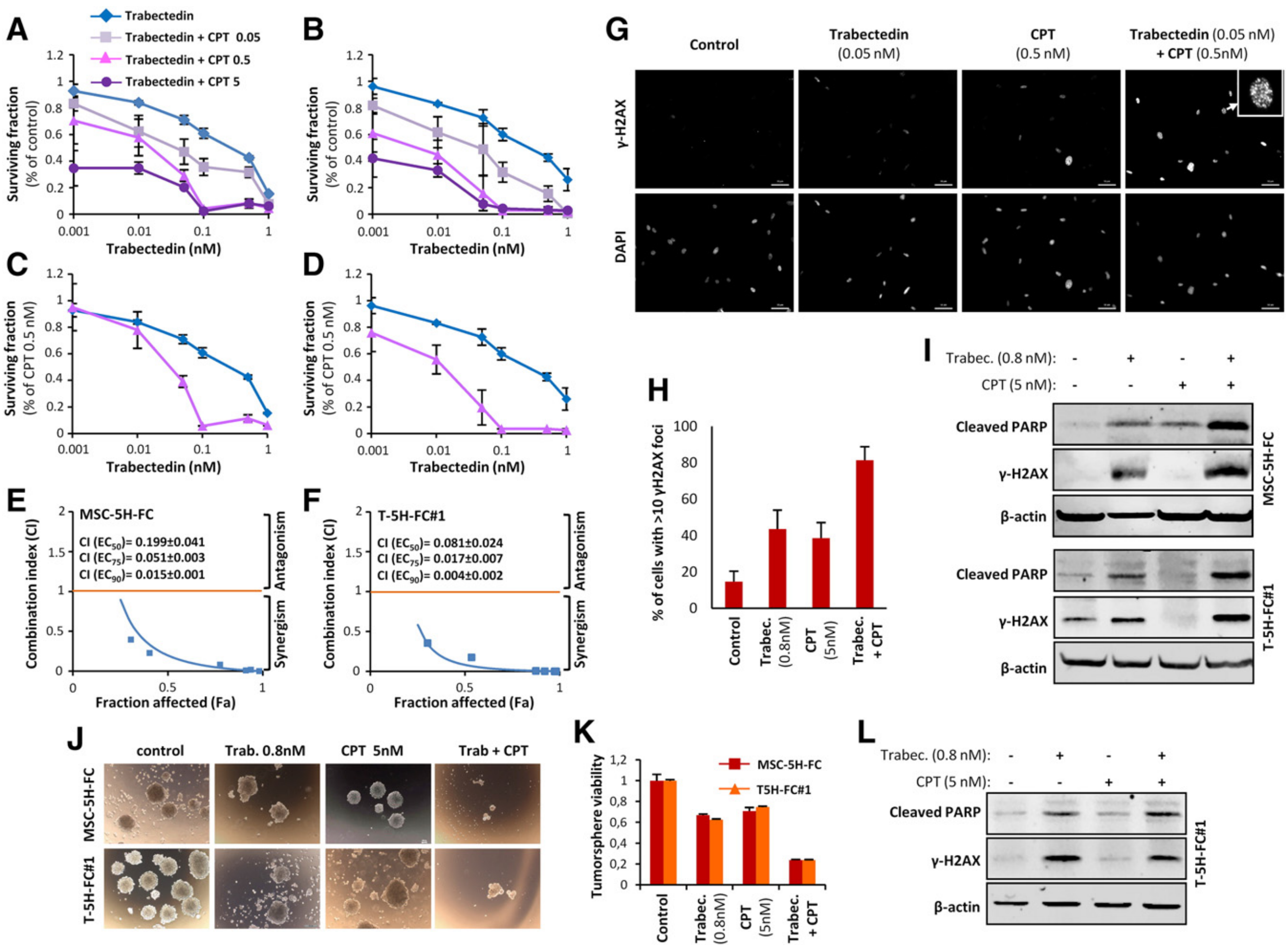

Figure 6. Trabectedin and camptothecin combination shows synergistic cytotoxic effect. (A-B) Dose–response curves of cell viability normalized to the solvent control at 72 h of treatment of MSC-5H-FC (A) or T-5H-FC#1 (B) cells with the indicated combination of drugs. (C-D) Dose–response cell viability curves of MSC-5H-FC (C) or T-5H-FC#1 (D) where the trabectedin + CPT series were normalized to the value observed after treatment with CPT alone. In this representation the effect of CPT alone is subtracted from the combination values, thus, showing the shift in the IC_{50} of trabectedin due to the combination. (E-F) Combination index plots generated for six constant ratio combinations of trabectedin and CPT (1:10) by the CompuSyn software according to the Chou-Talalay method. Most of the combinations meet the criteria for strong (CI between 0.1 and 0.3) and very strong synergism (CI <0.1). The CI values for ED_{50}, ED_{75} and ED_{90} combination doses as calculated by the median effect equation are shown. (G) Representative images of immunostaining experiments showing the effect of 1-hour treatment with trabectedin and/or CPT combination in γH2AX foci formation in MSC-5H cells. Inset shows a magnification of a representative cell. Scale bars = 50 μm. An enlarged color version of this panel is displayed as Figure S3B. (H) Quantification of γH2AX foci performed by counting cells high levels of DNA damage (>10 foci). More than 200 cells were counted for each condition. A similar set of experiments for T-5H-FC#1 cells is presented as Figure S4. (I) γH2AX, cleaved PARP and β-actin protein levels after the treatment of adherent cultures of MSC-5H and T-5H-FC#1 cells for 24 hours with the indicated concentrations. (J-K) MSC-5H-FC and T-5H-FC#1 cells were pre-treated with the indicated concentrations of trabectedin for 72 h and left to grow in tumorsphere culture conditions for 10 days. Representative images (J) and relative quantification of the cell viability (WST-1 assay) (K) are shown. Scale bars = 200 μm. (L) γH2AX, cleaved PARP and β-actin protein levels after the treatment of sphere cultures of T-5H-FC#1 cells for 24 hours with the indicated concentrations. Error bars represent the standard deviation of at least three independent experiments.

References

[1] Desar IM, Constantinidou A, Kaal SE, Jones RL, and van der Graaf WT (2016). Advanced soft-tissue sarcoma and treatment options: critical appraisal of trabectedin. *Cancer Manag Res* **8**, 95–104.

[2] Rodriguez R, Rubio R, and Menendez P (2012). Modeling sarcomagenesis using multipotent mesenchymal stem cells. *Cell Res* **22**, 62–77.

[3] Xiao W, Mohseny AB, Hogendoorn PC, and Cleton-Jansen AM (2013). Mesenchymal stem cell transformation and sarcoma genesis. *Clin Sarcoma Res* **3**, 10.

[4] Funes JM, Quintero M, Henderson S, Martinez D, Qureshi U, Westwood C, Clements MO, Bourboulia D, Pedley RB, and Moncada S, et al (2007). Transformation of human mesenchymal stem cells increases their dependency on oxidative phosphorylation for energy production. *Proc Natl Acad Sci U S A* **104**, 6223–6228.

[5] Rodriguez R, Rosu-Myles M, Arauzo-Bravo M, Horrillo A, Pan Q, Gonzalez-Rey E, Delgado M, and Menendez P (2014). Human bone marrow stromal cells lose immunosuppressive and anti-inflammatory properties upon oncogenic transformation. *Stem Cell Rep* **3**, 606–619.

[6] Rodriguez R, Tornin J, Suarez C, Astudillo A, Rubio R, Yauk C, Williams A, Rosu-Myles M, Funes JM, and Boshoff C, et al (2013). Expression of FUS-CHOP fusion protein in immortalized/transformed human mesenchymal stem cells drives mixoid liposarcoma formation. *Stem Cells* **31**, 2061–2072.

[7] De Sanctis R, Marrari A, and Santoro A (2016). Trabectedin for the treatment of soft tissue sarcomas. *Expert Opin Pharmacother* **17**, 1569–1577.

[8] Larsen AK, Galmarini CM, and D'Incalci M (2016). Unique features of trabectedin mechanism of action. *Cancer Chemother Pharmacol* **77**, 663–671.

[9] D'Incalci M and Galmarini CM (2010). A review of trabectedin (ET-743): a unique mechanism of action. *Mol Cancer Ther* **9**, 2157–2163.

[10] Germano G, Frapolli R, Belgiovine C, Anselmo A, Pesce S, Liguori M, Erba E, Uboldi S, Zucchetti M, and Pasqualini F, et al (2013). Role of macrophage targeting in the antitumor activity of trabectedin. *Cancer Cell* **23**, 249–262.

[11] Di Giandomenico S, Frapolli R, Bello E, Uboldi S, Licandro SA, Marchini S, Beltrame L, Brich S, Mauro V, and Tamborini E, et al (2014). Mode of action of trabectedin in myxoid liposarcomas. *Oncogene* **33**, 5201–5210.

[12] Forni C, Minuzzo M, Virdis E, Tamborini E, Simone M, Tavecchio M, Erba E, Grosso F, Gronchi A, and Aman P, et al (2009). Trabectedin (ET-743) promotes differentiation in myxoid liposarcoma tumors. *Mol Cancer Ther* **8**, 449–457.

[13] Grohar PJ, Griffin LB, Yeung C, Chen QR, Pommier Y, Khanna C, Khan J, and Helman LJ (2011). Ecteinascidin 743 interferes with the activity of EWS-FLI1 in Ewing sarcoma cells. *Neoplasia* **13**, 145–153.

[14] Grosso F, Jones RL, Demetri GD, Judson IR, Blay JY, Le Cesne A, Sanfilippo R, Casieri P, Collini P, and Dileo P, et al (2007). Efficacy of trabectedin (ecteinascidin-743) in advanced pretreated myxoid liposarcomas: a retrospective study. *Lancet Oncol* **8**, 595–602.

[15] Charytonowicz E, Terry M, Coakley K, Telis L, Remotti F, Cordon-Cardo C, Taub RN, and Matushansky I (2012). PPARgamma agonists enhance ET-743-induced adipogenic differentiation in a transgenic mouse model of myxoid round cell liposarcoma. *J Clin Invest* **122**, 886–898.

[16] Frapolli R, Tamborini E, Virdis E, Bello E, Tarantino E, Marchini S, Grosso F, Sanfilippo R, Gronchi A, and Tercero JC, et al (2010). Novel models of myxoid liposarcoma xenografts mimicking the biological and pharmacologic features of human tumors. *Clin Cancer Res* **16**, 4958–4967.

[17] Germano G, Frapolli R, Simone M, Tavecchio M, Erba E, Pesce S, Pasqualini F, Grosso F, Sanfilippo R, and Casali PG, et al (2010). Antitumor and anti-inflammatory effects of trabectedin on human myxoid liposarcoma cells. *Cancer Res* **70**, 2235–2244.

[18] Feuerhahn S, Giraudon C, Martinez-Diez M, Bueren-Calabuig JA, Galmarini CM, Gago F, and Egly JM (2011). XPF-dependent DNA breaks and RNA polymerase II arrest induced by antitumor DNA interstrand crosslinking-mimetic alkaloids. *Chem Biol* **18**, 988–999.

[19] Herrero AB, Martin-Castellanos C, Marco E, Gago F, and Moreno S (2006). Cross-talk between nucleotide excision and homologous recombination DNA repair pathways in the mechanism of action of antitumor trabectedin. *Cancer Res* **66**, 8155–8162.

[20] Soares DG, Escargueil AE, Poindessous V, Sarasin A, de Gramont A, Bonatto D, Henriques JA, and Larsen AK (2007). Replication and homologous recombination repair regulate DNA double-strand break formation by the antitumor alkylator ecteinascidin 743. *Proc Natl Acad Sci U S A* **104**, 13062–13067.

[21] Soares DG, Machado MS, Rocca CJ, Poindessous V, Ouaret D, Sarasin A, Galmarini CM, Henriques JA, Escargueil AE, and Larsen AK (2011). Trabectedin and its C subunit modified analogue PM01183 attenuate nucleotide excision repair and show activity toward platinum-resistant cells. *Mol Cancer Ther* **10**, 1481–1489.

[22] Damia G, Silvestri S, Carrassa L, Filiberti L, Faircloth GT, Liberi G, Foiani M, and D'Incalci M (2001). Unique pattern of ET-743 activity in different cellular systems with defined deficiencies in DNA-repair pathways. *Int J Cancer* **92**, 583–588.

[23] Takebayashi Y, Pourquier P, Zimonjic DB, Nakayama K, Emmert S, Ueda T, Urasaki Y, Kanzaki A, Akiyama SI, and Popescu N, et al (2001). Antiproliferative activity of ecteinascidin 743 is dependent upon transcription-coupled nucleotide-excision repair. *Nat Med* **7**, 961–966.

[24] Tavecchio M, Simone M, Erba E, Chiolo I, Liberi G, Foiani M, D'Incalci M, and Damia G (2008). Role of homologous recombination in trabectedin-induced DNA damage. *Eur J Cancer* **44**, 609–618.

[25] Takebayashi Y, Pourquier P, Yoshida A, Kohlhagen G, and Pommier Y (1999). Poisoning of human DNA topoisomerase I by ecteinascidin 743, an anticancer drug that selectively alkylates DNA in the minor groove. *Proc Natl Acad Sci U S A* **96**, 7196–7201.

[26] Grohar PJ, Segars LE, Yeung C, Pommier Y, D'Incalci M, Mendoza A, and Helman LJ (2014). Dual targeting of EWS-FLI1 activity and the associated DNA damage response with trabectedin and SN38 synergistically inhibits Ewing sarcoma cell growth. *Clin Cancer Res* **20**, 1190–1203.

[27] Ordonez JL, Amaral AT, Carcaboso AM, Herrero-Martin D, del Carmen Garcia-Macias M, Sevillano V, Alonso D, Pascual-Pasto G, San-Segundo L, and Vila-Ubach M, et al (2015). The PARP inhibitor olaparib enhances the sensitivity of Ewing sarcoma to trabectedin. *Oncotarget* **6**, 18875–18890.

[28] Riccardi A, Meco D, Ubezio P, Mazzarella G, Marabese M, Faircloth GT, Jimeno J, D'Incalci M, and Riccardi R (2005). Combination of trabectedin and irinotecan is highly effective in a human rhabdomyosarcoma xenograft. *Anticancer Drugs* **16**, 811–815.

[29] Cosetti M, Wexler LH, Calleja E, Trippett T, LaQuaglia M, Huvos AG, Gerald W, Healey JH, Meyers PA, and Gorlick R (2002). Irinotecan for pediatric solid tumors: the Memorial Sloan-Kettering experience. *J Pediatr Hematol Oncol* **24**, 101–105.

[30] Monterrubio C, Pascual-Pasto G, Cano F, Vila-Ubach M, Manzanares A, Schaiquevich P, Tornero JA, Sosnik A, Mora J, and Carcaboso AM (2016). SN-38-loaded nanofiber matrices for local control of pediatric solid tumors after subtotal resection surgery. *Biomaterials* **79**, 69–78.

[31] Wagner L (2011). Camptothecin-based regimens for treatment of ewing sarcoma: past studies and future directions. *Sarcoma* **2011**, 957957.

[32] Zeng FY, Cui J, Liu L, and Chen T (2009). PAX3-FKHR sensitizes human alveolar rhabdomyosarcoma cells to camptothecin-mediated growth inhibition and apoptosis. *Cancer Lett* **284**, 157–164.

[33] Pommier Y (2006). Topoisomerase I inhibitors: camptothecins and beyond. *Nat Rev Cancer* **6**, 789–802.

[34] Rodriguez R, Hansen LT, Phear G, Scorah J, Spang-Thomsen M, Cox A, Helleday T, and Meuth M (2008). Thymidine selectively enhances growth suppressive effects of camptothecin/irinotecan in MSI+ cells and tumors containing a mutation of MRE11. *Clin Cancer Res* **14**, 5476–5483.

[35] Rodriguez R, Rubio R, Gutierrez-Aranda I, Melen GJ, Elosua C, Garcia-Castro J, and Menendez P (2011). FUS-CHOP fusion protein expression coupled to p53 deficiency induces liposarcoma in mouse but not in human adipose-derived mesenchymal stem/stromal cells. *Stem Cells* **29**, 179–192.

[36] Rubio R, Gutierrez-Aranda I, Saez-Castillo AI, Labarga A, Rosu-Myles M, Gonzalez-Garcia S, Toribio ML, Menendez P, and Rodriguez R (2013). The differentiation stage of p53-Rb-deficient bone marrow mesenchymal stem cells imposes the phenotype of in vivo sarcoma development. *Oncogene* **32**, 4970–4980.

[37] Martinez-Cruzado L, Tornin J, Santos L, Rodriguez A, Garcia-Castro J, Moris F, and Rodriguez R (2016). Aldh1 Expression and Activity Increase During Tumor Evolution in Sarcoma Cancer Stem Cell Populations. *Sci Rep* **6**, 27878.

[38] Tornin J, Martinez-Cruzado L, Santos L, Rodriguez A, Nunez LE, Oro P, Hermosilla MA, Allonca E, Fernandez-Garcia MT, and Astudillo A, et al (2016). Inhibition of SP1 by the mithramycin analog EC-8042 efficiently targets tumor initiating cells in sarcoma. *Oncotarget* **7**, 30935–30950.

[39] Chou TC (2006). Theoretical basis, experimental design, and computerized simulation of synergism and antagonism in drug combination studies. *Pharmacol Rev* **58**, 621–681.

[40] Rubio R, Abarrategi A, Garcia-Castro J, Martinez-Cruzado L, Suarez C, Tornin J, Santos L, Astudillo A, Colmenero I, and Mulero F, et al (2014). Bone environment is essential for osteosarcoma development from transformed mesenchymal stem cells. *Stem Cells* **32**, 1136–1148.

[41] Kaufmann SH, Peereboom D, Buckwalter CA, Svingen PA, Grochow LB, Donehower RC, and Rowinsky EK (1996). Cytotoxic effects of topotecan combined with various anticancer agents in human cancer cell lines. *J Natl Cancer Inst* **88**, 734–741.

[42] Pourquier P, Waltman JL, Urasaki Y, Loktionova NA, Pegg AE, Nitiss JL, and Pommier Y (2001). Topoisomerase I-mediated cytotoxicity of N-methyl-N'-nitro-N-nitrosoguanidine: trapping of topoisomerase I by the O6-methylguanine. *Cancer Res* **61**, 53–58.

[43] Acikgoz E, Guven U, Duzagac F, Uslu R, Kara M, Soner BC, and Oktem G (2015). Enhanced G2/M Arrest, Caspase Related Apoptosis and Reduced E-Cadherin Dependent Intercellular Adhesion by Trabectedin in Prostate Cancer Stem Cells. *PLoS One* **10**, e0141090.

[44] Blay JY, Leahy MG, Nguyen BB, Patel SR, Hohenberger P, Santoro A, Staddon AP, Penel N, Piperno-Neumann S, and Hendifar A, et al (2014). Randomised phase III trial of trabectedin versus doxorubicin-based chemotherapy as first-line therapy in translocation-related sarcomas. *Eur J Cancer* **50**, 1137–1147.

[45] Mannarino L, Paracchini L, Craparotta I, Romano M, Marchini S, Gatta R, Erba E, Clivio L, Romualdi C, and D'Incalci M, et al (2016). A systems biology approach to investigate the mechanism of action of trabectedin in a model of myelomonocytic leukemia. *Pharm J* .

[46] Herzog J, von Klot-Heydenfeldt F, Jabar S, Ranft A, Rossig C, Dirksen U, Van den Brande J, D'Incalci M, von Luettichau I, and Grohar PJ, et al (2016). Trabectedin Followed by Irinotecan Can Stabilize Disease in Advanced Translocation-Positive Sarcomas with Acceptable Toxicity. *Sarcoma* **2016**, 7461783.

[47] Tancredi R, Zambelli A, DaPrada GA, Fregoni V, Pavesi L, Riccardi A, Burdach S, Grohar PJ, and D'Incalci M (2015). Targeting the EWS-FLI1 transcription factor in Ewing sarcoma. *Cancer Chemother Pharmacol* **75**, 1317–1320.

[48] Kawano M, Mabuchi S, Kishimoto T, Hisamatsu T, Matsumoto Y, Sasano T, Takahashi R, Sawada K, Takahashi K, and Takahashi T, et al (2014). Combination treatment with trabectedin and irinotecan or topotecan has synergistic effects against ovarian clear cell carcinoma cells. *Int J Gynecol Cancer* **24**, 829–837.

[49] Shamanna RA, Lu H, Croteau DL, Arora A, Agarwal D, Ball G, Aleskandarany MA, Ellis IO, Pommier Y, and Madhusudan S, et al (2016). Camptothecin targets WRN protein: mechanism and relevance in clinical breast cancer. *Oncotarget* **7**, 13269–13284.

[50] Takebayashi Y, Goldwasser F, Urasaki Y, Kohlhagen G, and Pommier Y (2001). Ecteinascidin 743 induces protein-linked DNA breaks in human colon carcinoma HCT116 cells and is cytotoxic independently of topoisomerase I expression. *Clin Cancer Res* **7**, 185–191.